ISTANBUL UNIVERSITY –
JOURNAL OF ELECTRICAL & ELECTRONICS ENGINEERING

YEAR : 2004 (1007-1016)
VOLUME : 4
NUMBER : 1

GLOBAL OPTIMIZATION OF OPTICAL FLOW TECHNIQUE ON THE COMPUTATION OF TISSUE-MOTION IN NEONATAL CRANIAL ULTRASONOGRAM

Mohiuddin AHMAD[1] M. S. YUSUF[2] M. Z. CHOWDHURY[3] M. YAMADA[4]

[1, 2, 3] Dept. of Electrical & Electronic Engineering, Bangladesh Institute of Technology (BIT), Khulna, Bangladesh
[4] Dept. of Electronics and Information Science, Kyoto Institute of Technology, Japan

E-mail: mohi_bitk@yahoo.com

ABSTRACT

In this paper, a global optimization method of optical flow technique is presented for estimating tissue-motion velocity from a time series of neonatal cranial ultrasonogram images. The global optimization method is used here was proposed by Horn and Schunck. In this method, the tissue-motion velocity field is determined by minimizing an error function based on the gradient constraint and a global smoothing term over the whole image. An iterative implementation is shown which successfully computes the tissue-motion velocity for a number of cranial ultrasonogram image sequences. Two dimensional tissue-motion vectors are presented, shows that artery pulsation can be detected in low brightness image. It is shown that, the strength of artery pulsation can be quantitatively estimated by using the magnitude of tissue motion vector.

Keywords: *optical flow, global optimization, tissue-motion, ultrasonogram, newborn baby.*

I. INTRODUCTION

Ultrasonogram imaging systems have become widely used tools in many medical applications. As an example, it is widely used in observing different organs in human body due to its convenience, easy to use and low cost. In general, medical doctors record observations as stationary images for medical diagnosis. Observations are also recoded as moving images in videotapes as ultrasonographic movie for future diagnosis. In case of newborn baby, the pediatricians observe the brain tissue by ultrasonogram. In this case they use the ultrasonographic movie to detect cranial abnormalities in newborn babies, since they can observe the brain tissue through anterior fontanelle [2], [8].

Tissue-motion of an ultrasonographic image sequence is an important parameter since it can be considered as the strength of artery pulsation of a newborn baby head. The brain tissues experience motions due to blood flow to the brain. The velocity experience by brain tissue is known as tissue-motion velocity. The nature of tissue motion velocity is periodic due to periodic nature of heartbeat [13]. Since the heartbeat varies due to physical condition of newborn babies, the tissue-motion velocities vary from time to time, baby to baby.

Artery pulsation is the periodic beating of arteries as blood is pumped through arteries. The

Received Date : 03.03.2003
Accepted Date: 05.10.2003

strength of artery pulsation represents the rating of blood flow through arteries. The tissue-motion velocity is associated with blood flow [2], [6], [13]. Therefore, the strength of artery pulsation can be considered as the magnitude of tissue-motion velocity. The main point of pediatric diagnosis is the intensity of pulsation associated with blood flow [2], [13]. Therefore detection of pulsation and quantitative recognition of artery pulsation are good issues for pediatric diagnosis.

In this paper, we study the tissue-motion detection and computation due to artery pulsation in neonatal cranial ultrasonogram by using global optimization method of optical flow technique. This is very helpful for quantitative characterization of artery pulsation. Tissue-motion velocity image and two-dimensional mapping of tissue-motion vectors are presented; emphasizing that artery pulsation can be detected even in low brightness image. It is also demonstrated that strength of artery pulsation can be quantitatively estimated by using the tissue-motion vector.

II. OPTICAL FLOW TECHNIQUE

Optical flow is a method for computing a motion field and has been employed mostly in the computer vision and artificial intelligence community since 1970s. By definition, optical flow is a dense velocity vector field that represents the motion of brightness patterns between successive frames. It has been widely used in computer vision to provide important cues for motion and vision analysis.

The neonatal cranial ultrasonogram is taken as noisy, speckle-like grayscale image including non-rigid tissues such as cerebrums and arteries with local motion due to pulsation of blood flow [6]. Therefore, the tissue-motions may vary with time and place. We suppose that the tissue like artery in echo image is locally rigid and keeps its texture during instantaneous motion. In order to calculate the tissue-motion velocity as the instantaneous optical flow at any pixel over the whole ultrasonographic region, a gradient-based approach combined with global optimization is used. In global optimization method, the tissue-motion velocity field is determined by minimizing an error function based on the gradient constraint and a global smoothing term over the whole image [1], [10]. Gradient-based approaches provide a solution to motion estimation from the observation in time of changes in the image brightness [7]. These changes are modeled by means of partial differential equations, which are called *constraint equations*. The field of velocity vector obtained by solving such partial differential equations is normally called as optical flow or image flow [7]. In this paper, it is defined as tissue-motion velocity.

Let $p(x, y, t)$ be the image function as brightness in an ultrasound image sequence of a moving point (x, y) and at a time t. If the point moves to another point $(x + \delta x, y + \delta y)$ after a short duration δt and the brightness of the point doesn't change over the time δt , then we can formulate

$$p(x + \delta x, y + \delta y, t + \delta t) = p(x, y, t) \quad (1)$$

Expanding left hand side of Eq. (1) in a Taylor series around the point (x, y, t) and taking the limit of its first-order components as $\delta t \to 0$, the gradient constraint equation [1], [9], [3], [4], [7], [13] is obtained.

$$\frac{\partial p}{\partial x}\frac{dx}{dt} + \frac{\partial p}{\partial y}\frac{dy}{dt} + \frac{\partial p}{\partial t} = 0 \quad (2)$$

Or, simply, we can write

$$p_x v_x + p_y v_y + p_t = 0 \quad (3)$$

Here, $p_x = \partial p / \partial x$, $p_y = \partial p / \partial y$ are spatial gradients and $p_t = \partial p / \partial t$ is temporal gradient. $\partial p / \partial t$ at a given pixel is just how fast the brightness or intensity is changing with time, while $\partial p / \partial x$ and $\partial p / \partial y$ are the spatial rates of change of image brightness or intensity , i.e. how rapidly brightness changes on going across the picture , so all three of these quantities can be estimated for each pixel by considering the images.

The x and y components of optical flow velocity or tissue-motion velocity, $\vec{v} = (v_x, v_y)$ are defined as follows:

$$v_x = \frac{dx}{dt}, \quad v_y = \frac{dy}{dt} \tag{4}$$

Equation (3) is called the motion constraint equation or optical flow constraint (OFC) equation [12] to solve for $\vec{v} = (v_x, v_y)$, since it expresses a constraint on the components v_x and v_y of the optical flow.

The OFC equation can be written as

$$(p_x, p_y) \cdot (v_x, v_y) = -p_t \tag{5}$$

Thus the component of the tissue-motion velocity in the direction of image brightness gradient at the image of a pixel point is

$$(v_x, v_y) = -\frac{-p_t}{\sqrt{p_x^2 + p_y^2}} \tag{6}$$

We cannot however, determine the component of the optical flow at right angles to this direction. This ambiguity is known as *aperture problem*.

Global or local optimization technique can be used to overcome this problem. Global optimization technique is adopted in this paper.

A. *Global Optimization Method*

Global optimization has been used to develop many vision algorithms for early vision processing, although it is very difficult to solve a global optimization problem. Global optimization method plays more preferable to estimate motion over local optimization problem for the following advantages; all local optimization techniques can at most locate a local minimum but not global, there is no local criterion to decide whether a local solution is the global solution and locally optimal solutions often prove insufficient for real world engineering problems.

In the global optimization methods, a functional is defined where a smoothness constraint is used to regularize the solution of a partial differential equation and the influence of the smoothness constraint is weighted with a positive constant [7]. The functional is minimized by calculus of variations or stochastic relaxation [7].

We follow the approach of Horn and Schunck [1] for solving the underdetermined optical flow problem. Horn and Schunck [1] formulated an optimization problem for estimating optical flow. The optimization measure consisted of two terms:

(i) A penalty on the deviation of the estimated velocity field from the image flow constraint equation and

(ii) A penalty on the deviation of the velocity field components from smoothing surfaces. The smoothness penalty is the sum of the squares of the magnitude of the gradient of image flow velocity or simply divergence of velocity field.

According to above definition, we construct a total error measure $\varepsilon^2(\alpha)$ as the spatial integral of two terms, ε_0^2 and ε_s^2 where,

$$\varepsilon^2(\alpha) = \iint_{image} \left(\varepsilon_0^2(x,y,t) + \alpha^2 \varepsilon_s^2(x,y,t)\right) dx dy \tag{7}$$

where

(i) $\varepsilon_0^2(x,y,t) = (p_x v_x + p_y v_y + p_t)^2$: Square of the error from the OFC, and

(ii) $\varepsilon_s^2(x,y,t) = \left(\frac{\partial v_x}{\partial x}\right)^2 + \left(\frac{\partial v_y}{\partial x}\right)^2 + \left(\frac{\partial v_x}{\partial y}\right)^2 + \left(\frac{\partial v_y}{\partial y}\right)^2$: Penalty that encourages smoothness

α is a regularization coefficient or weighting factor that controls the influence of the smoothness constraint. The error function is minimized by using the calculus of variations. From minimization, we obtain a system of two coupled differential equations from the Euler-Lagrange equations [7], [10].

$$\begin{aligned} \nabla^2 v_x &= \frac{p_x}{\alpha^2}(p_x v_x + p_y v_y + p_t) \\ \nabla^2 v_y &= \frac{p_y}{\alpha^2}(p_x v_x + p_y v_y + p_t) \end{aligned} \tag{8}$$

∇^2 is the *Laplacian operator*, $\nabla^2 = \frac{\partial^2}{\partial x^2} + \frac{\partial^2}{\partial y^2}$

We approximate the Laplacian of v_x, v_y by

$$\begin{aligned} \nabla^2 v_x &\approx \bar{v}_{x(i,j,k)} - v_{x(i,j.k)} \\ \nabla^2 v_y &\approx \bar{v}_{y(i,j,k)} - v_{y(i,j.k)} \end{aligned} \tag{9}$$

where $\bar{v}_{x(i,j,k)}$ and $\bar{v}_{y(i,j,k)}$ denote Gaussian weighted average of the neighbor points around the point at pixel position (i, j, k).

The local averages $\bar{v}_{x(i,j,k)}$ and $\bar{v}_{y(i,j,k)}$ are defined as follows [1], [7]:

$$\begin{aligned} \bar{v}_{x(i,j,k)} &= (v_{x(i-1,j-1,k)} + v_{x(i-1,j+1,k)} + v_{x(i+1,j-1,k)} + v_{x(i+1,j+1,k)})/12 \\ &+ (v_{x(i-1,j,k)} + v_{x(i+1,j,k)} + v_{x(i,j-1,k)} + v_{x(i,j+1,k)})/6 \end{aligned} \tag{10.a}$$

$$\begin{aligned} \bar{v}_{y(i,j,k)} &= (v_{y(i-1,j-1,k)} + v_{y(i-1,j+1,k)} + v_{y(i+1,j-1,k)} + v_{y(i+1,j+1,k)})/12 \\ &+ (v_{y(i-1,j,k)} + v_{y(i+1,j,k)} + v_{y(i,j-1,k)} + v_{y(i,j+1,k)})/6 \end{aligned} \tag{10.b}$$

Combining Eq. (8) with Eq. (9) and isolating v_x and v_y leads to

$$v_x = \bar{v}_x - \frac{p_x[p_x\bar{v}_x + p_y\bar{v}_y + p_t]}{\alpha^2 + p_x^2 + p_y^2} \tag{11.a}$$

$$v_y = \bar{v}_y - \frac{p_y[p_x\bar{v}_x + p_y\bar{v}_y + p_t]}{\alpha^2 + p_x^2 + p_y^2} \tag{11.b}$$

Equation (11) is a system of linear equations with about 10^7 variables. For estimating the velocity, direct matrix methods such as Gauss-Jordan are computationally expensive, so we use iterative method such as Gauss-Seidel method [5], [11]. If the velocity estimates are $v_{x(i,j,k)}^{n+1}$, $v_{y(i,j,k)}^{n+1}$ and the average of previous velocity estimates are $(v_x^{\,n}, v_y^{\,n})$, where n denotes iteration number, then the estimated velocity at any pixel position (i, j, k) is given by [1], [9].

$$v_{x(i,j,k)}^{n+1} = \bar{v}_{x(i,j,k)}^{n} - \frac{p_{x(i,j,k)}[p_{x(i,j,k)}\bar{v}_{x(i,j,k)}^{n} + p_{y(i,j,k)}\bar{v}_{y(i,j,k)}^{n} + p_{t(i,j,k)}]}{\alpha^2 + p_{x(i,j,k)}^2 + p_{y(i,j,k)}^2} \tag{12.a}$$

$$v^{n+1}_{y(i,j,k)} = \bar{v}^{n}_{y(i,j,k)} - \frac{p_{y(i,j,k)}\left[p_{x(i,j,k)}\bar{v}^{n}_{x(i,j,k)} + p_{y(i,j,k)}\bar{v}^{n}_{y(i,j,k)} + p_{t(i,j,k)}\right]}{\alpha^2 + p^2_{x(i,j,k)} + p^2_{y(i,j,k)}} \tag{12.b}$$

p_x, p_y and p_t are approximations to the derivative and computed by averaging finite element differentials in three consecutive input images from cranial ultrasonographic movie. At any iteration, the absolute value of tissue-motion velocity, $|V|_{(i,j,k)}$ and the phase angle $\phi_{(i,j,k)}$ of velocity at each pixel position (i,j,k) are given by

$$|V|_{(i,j,k)} = \sqrt{v^2_{x(i,j,k)} + v^2_{y(i,j,k)}}\ ,\ \phi_{(i,j,k)} = \tan^{-1}\frac{v_{y(i,j,k)}}{v_{x(i,j,k)}} \tag{13}$$

B. ***Average value and Standard deviation of Motion***

The average value, $\overline{|V|}_{(i,j)}$ and standard deviation, $\sigma_{|V|_{(i,j)}}$ of tissue-motion velocity is calculated over n number of frames within the ROI at any pixel position (i,j) are given by the following equations:

$$\overline{|V|}_{(i,j)} = \sum_{k=1}^{n}\frac{|V|_{(i,j,k)}}{n} \tag{14}$$

$$\sigma_{|V|_{(i,j)}} = \sqrt{\sum_{k=1}^{n}\frac{|V|^2_{(i,j,k)}}{n} - \left(\sum\frac{|V|_{(i,j,k)}}{n}\right)^2} \tag{15}$$

Here, n is the number of frames used for calculation, which are 30.

C. ***Estimation of Gradients***

The derivative of image brightness is estimated from discrete pixel values. There are many formulas for approximating the differentiation. We have estimated the gradients at each pixel point (i,j,k) by central finite difference formulas [11] from three consecutive frames are shown in Eq. (16). In Fig. 1, the

$$p_x = \frac{1}{2}\left[p(i+1,j,k) - p(i-1,j,k)\right] \tag{16.a}$$

$$p_y = \frac{1}{2}\left[p(i,j+1,k) - p(i,j-1,k)\right] \tag{16.b}$$

$$p_t = \frac{1}{2}\left[p(i,j,k+1) - p(i,j,k-1)\right] \tag{16.c}$$

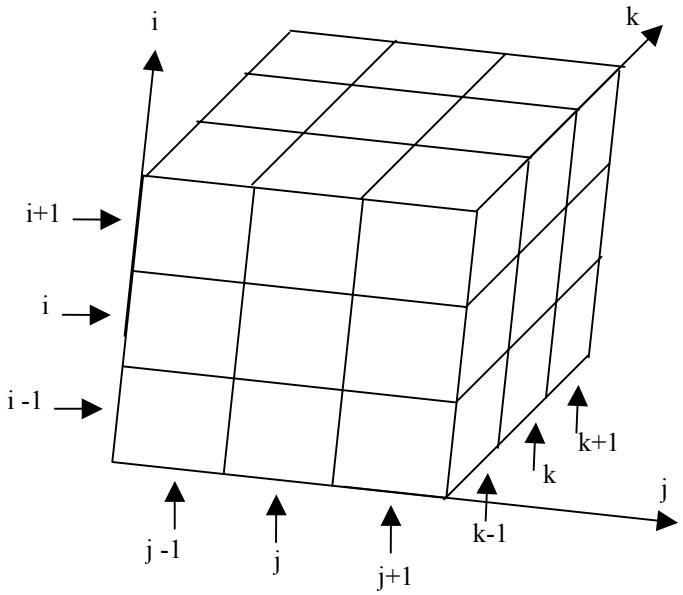

Fig. 1. Estimation of gradients from central finite difference along nine parallel edges of the cube.

relationship in space and time between these estimates are shown. Here the column index j corresponds to x-direction in the image, the row index i to the y-direction, while k lies in the time direction. It is important that the estimates of p_x, p_y and p_t be consistent [1]. That is, they should all refer to the same point in the image at the same time. Here the unit of length in the grid spacing interval in each image frame and the unit of time is the image frame-sampling period.

III. EXPERIMENTAL RESULTS AND DISCUSSION

For estimating tissue-motion velocity from neonatal cranial ultrasonogram, we use the ultrasonographic movie. The original ultrasonographic movie used here were taken in the brightness mode using an ultrasound probe of 5.0 MHz and recoded on videotapes at the site of pediatricians. Port Royal method [8] is used for sections scanned through the anterior fontanelle of the neonate. A PCI-based PC then captured a series of ultrasound echo images with video digitizer. The specification of the captured ultrasonographic movie is shown in table -1.

Table 1: Specification of the captured ultrasonogram movie

No. of frames	32
Frame resolution	640×480 pixels/frame
Depth of each pixel	8 bits/pixel
Frame rate	33 ms/frame

The tissue-motion velocity is then computed at each pixel by using global optimization of optical flow technique. We use almost 64 iterations for calculating the tissue-motion in global optimization method and $\alpha = 0.01$ because better results are produced by it. The initial velocity estimate v_x^0 and v_y^0 are set to zero. The experimental results are shown by using ultrasonographic image, tissue-motion velocity image with region of interest (ROI), histogram and two-dimensional tissue-motion vectors.

A. ***Neonatal Cranial Ultrasonogram***

Figure 2 shows the first frame of a series of cranial ultrasonographic images in the anterior coronal section.

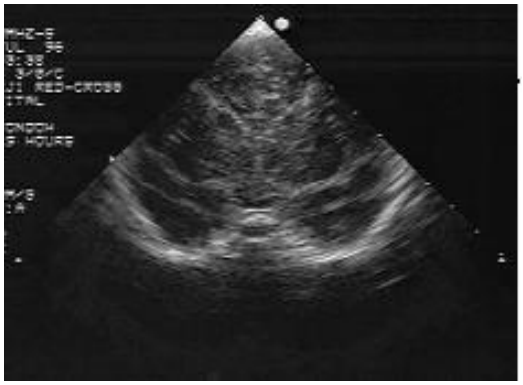

Fig. 2. Typical ultrasonographic image in the anterior coronal section of a neonatal cranium.

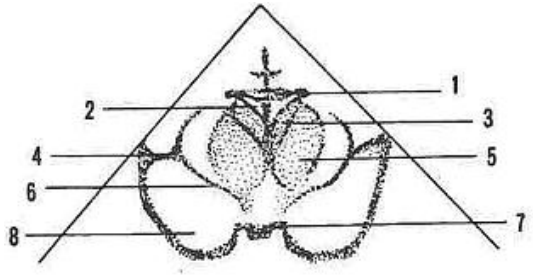

Fig.3. Essential tissue scheme in the anterior coronal section. 1: corpus callosum, 2: lateral ventricle, 3: head of caudate nucleus, 4: Sylvian fissure, 5: lenticular nucleus, 6: middle cerebral artery, 7: body of sphenoid bone, 8: temporal lobe

The ultrasonographic images were taken at the site of pediatricians. The left hand side of the figure corresponds to the right hand side of neonatal head. The detailed scheme of essential tissue in the anterior coronal sections [8] in typical neonatal cranial is shown in Fig. 3.

B. ***Tissue-motion Velocity Image***

Figure 4 shows the optical flow velocity as well as the tissue-motion velocity image in the first frame. This image is constructed from the absolute value of tissue-motion velocity. The image can be regarded as the pulsation image since artery pulsation can be represented by the magnitude of tissue-motion velocity. The white region shows the strong pulsation. Tissue-motion velocity is not observed in the region of cranial bone. It is observed that the distribution of tissue-motion velocity is not same within the entire image. In the original ultrasonographic image such pulsation is not observed like tissue-motion velocity image. Therefore, tissue-motion velocity image is useful to observe pulsation. Figure 5 shows the region of interest (ROI) corresponding to Fig. 4, which is considered for computing the average value and standard deviation of tissue-motion velocity. The ROI is chosen at the inside of cranial bone. Inside ROI, there are arteries and organs. Outside ROI, there are cranial bone and artifacts.

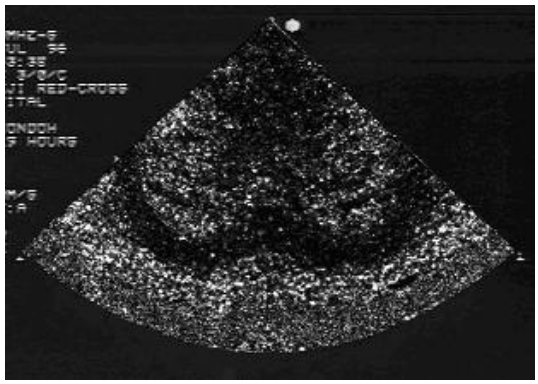

Fig.4. Tissue-motion velocity image corresponding the original ultrasonographic image

Fig.5. ROI of the tissue-motion velocity image corresponding to Fig. 3.

C. ***Histogram analysis of Tissue-motion Velocity***

Figures 6 and 7 show the histogram constructed by average value, $\overline{|V|}$ and standard deviation,

$\sigma_{|V|}$ of tissue-motion velocity versus relative items, n_i / N respectively. In these histograms, the differences of the distribution of tissue-motion velocity as well as pulsation between two babies are shown. The histogram gives the information on the relative items of occurrence of tissue-motion having various values of tissue-motion. In general, it is found that with increasing the value of tissue-motion, the relative number of items decreases. But some baby has strong pulsation than other baby. That means, the strength of artery pulsation is different for difference cases.

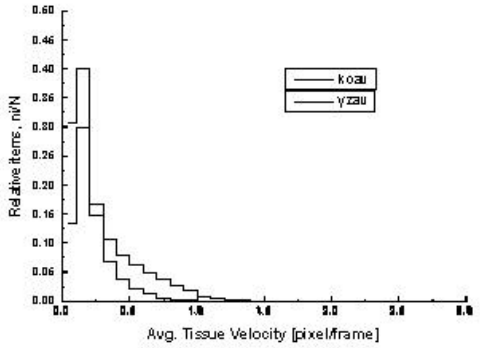

Fig. 6. Average tissue velocity versus relative items

The magnitude of the histogram at a specific tissue-motion velocity is the probability of the tissue-motion velocity occurring in the ultrasonographic movie. No information is given about the location of the velocity. The probability of the average value of tissue-motion velocity, $\overline{|V|}$ and standard deviation, $\sigma_{|V|}$ occurring at a given revalue within the ROI is given by

$$p\left(\overline{|V|}\right) = \overline{|V|} \times \frac{n_i}{N} \tag{17}$$

$$p\left(\sigma_{|V|}\right) = \sigma_{|V|} \times \frac{n_i}{N} \tag{18}$$

The shape of the histogram provides the information on the characteristics of the ultrasonographic movie within the ROI. A specific value of tissue-motion velocity may represent a unique characteristic of the item.

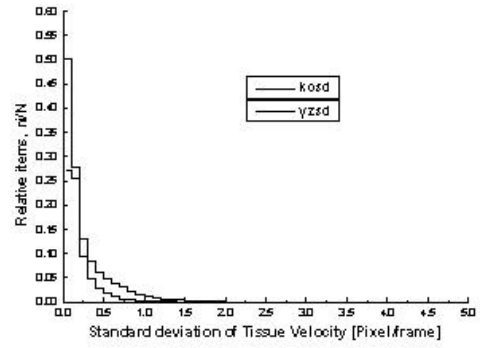

Fig. 7. Standard deviation of tissue velocity versus relative items

D. *Two-dimensional Distribution of Tissue-motion Velocity*

Two-dimensional velocity component (v_x, v_y) are computed from the cranial ultrasonographic movie for each pixel point and each time. We use 64 iterations for calculating the tissue-motion in global optimization method because of reaching the convergence and $\alpha = 0.1$ because better results are produced by it. A rectangle is considered in the original cranial

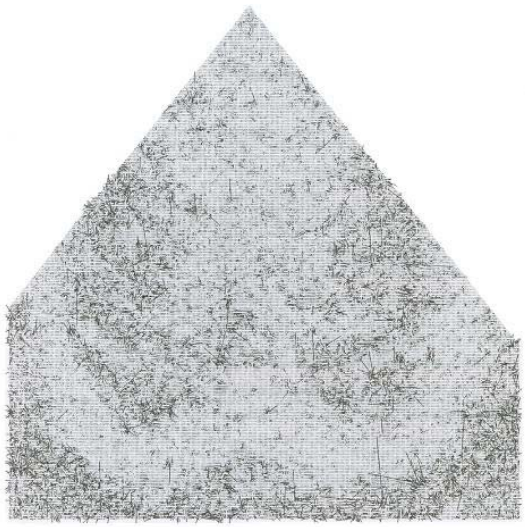

Fig.8. Two-dimensional maps of tissue-motion vectors in the anterior coronal section of neonatal cranial ultrasonographic image.

ultrasonographic movie and the tissue-motion velocity data (absolute value, phase angle) is taken for mapping the 2D velocity vectors of that rectangle.

Fig. 8. shows the two-dimensional map of tissue-motion vector of the a cranial ultrasonography, corresponding to Fig. 4. It should be noted here that we do not consider the motion vectors appeared on the outside of cranial bone. Also almost no motion vectors are found in the region of cranial bone. The magnitude of tissue-motion vector is normalized so that the distance between two neighbor pixels in the map is corresponded to 0.5 pixel/frame. It is observed that tissue-motion vectors vary with place and its magnitude becomes up to a few pixels/frame at several regions within the cranial bone. Furthermore, it is found that the maximum vectors are aligned to the same directions at many regions of the image.

The middle cerebral artery is one of the essential arteries and there are fine arteries around sylvian fissure and corpus callosum. The spatial distribution of large motion vectors is found in the above regions. On the other hand, the magnitude of motion vectors becomes zero on the cranial bone and at such tissues as lenticular nucleus.

The motion vectors are also calculated from the cranial ultrasonographic movie in different sections from the anterior coronal one, and they are confirmed to illustrate the same tendency as Fig. 8. Therefore, it can be concluded that the tissue-motion of artery pulsation is observed as the large motion vectors with the tendency to be aligned to the same directions in two-dimensional mapping of tissue-motion vectors.

The cranial ultrasonographic movies were also taken under the condition of low brightness in the same section as shown in Fig. 2. Two dimensional tissue-motion vectors are coincides with Fig. 8.

Therefore it can be confirmed that tissue-motion vectors is not affected by the spatial variation of brightness in ultrasonographic movie. This fact indicates that the pulsation strength can be quantitatively estimated by using the magnitude of tissue-motion velocity.

If the tissue-motion vectors can be computed and displayed in real time at the site of diagnosis, pediatricians can easily recognize the artery pulsations quantitatively because the tissue motion vectors proposed here is not affected by the spatial variation of brightness in cranial ultrasonographic image.

IV. CONCLUSIONS

The method proposed in this paper is based on Horn and Shunck's two dimensional optical flow measurement. In order to characterize artery pulsation quantitatively, the tissue-motion velocities are successfully computed at each pixel position due to artery pulsation by using the gradient-based method with global optimization. From different histogram it is found that the strength of artery pulsation as well as the distribution of pulsation is different. Since tissue-motion is not affected by the spatial variation of image brightness, therefore the strength of artery pulsation can be quantitatively estimated by using the magnitude of tissue-motion velocity. From tissue-motion velocity image pulsation is observed clearly, which will be helpful for pediatricians.

REFERENCES

[1] B. K. P. Horn, and B.G. Schunck, Determining Optical Flow, *Artificial Intelligence* 17, pp.185-203, 1981.

[2] M. Yamada, M. Fukuzawa, Y. Kitsunezuka, J. Kishida, N. Nakamori, H. Kanamori, T. Sakurai and S. Kodama, "Pulsation detection from noisy ultrasound echo moving images of newborn baby head using Fourier transform," *Jpn. J. Appl. Phys*., vol:34, pp. 2854-2856, 1995.

[3] J. K. Kearney, W. B. Thompson, and D. L. Boley, Optical Flow Estimation: An Error Analysis of Gradient-Based Methods with Local Optimization, *IEEE Transactions on Pattern Analysis and Machine intelligence*, Vol: 9, pp.229-244, March 1987.

[4] M. Ahmad and M. Yamada, "Notes on Gradient-Based Methods for Estimation of Tissue-motion Velocity in Ultrasound Image Sequences", *Journal of Electrical Engineering, the Institution of*

Engineers (JEE), vol: EE29, No: 1, pp. 13-18, June 2001.

[5] William H. Press, Saul A. Teukolsky, William T. Vetterling and Brian P. Flannery, "Numerical Recipes in C: The art of Scientific Computing", Second Edition, Cambridge University press.

[6] M. Fukuzawa, H. Kubo, Y. Kitsunezuka, and M. Yamada, Motion analysis of artery pulsation in neonatal cranial ultrasonogram, *SPIE,* vol. 3661, 1999.

[7] P. Laplante, and A. D. Stoyenko, Real-Time Imaging: Theory, Techniques, and Applications, *IEEE press*, 1996.

[8] Y.Kitsunezuka, and H. Nakamura, *Syonika-Rinsyo*, 38, pp. 297-308 [in Japanese], 1985.

[9] J. L. Barron, D.J. Fleet and S. S. Beauchemin, "Performance of Optical flow Techniques," *International Journal of Computer Vision*, vol. 12 no.1, pp. 43-77, 1994.

[10] "A volumetric Optical flow Method for Measurement of Brain Deformation from Intraoperative Magnetic Resonance Images," http://www.spl/harvard/edu

[11] Steven C. Chapara and Raymond P. Canale, "Numerical methods for Engineers – with Programming and Software Applications" Third edition, McGraw Hill International editions, 1998.

[12] H.H. Nagel, On the Estimation of Optical Flow: Relations between Different Approaches and Some New Results, Artificial *Intelligence*, vol.33, pp.299-324, January 1987.

[13] Mohiuddin Ahmad, "Optical flow analysis of Tissue-motion in cranial ultrasonogram of newborn baby" – *M. Engineering Thesis*, Kyoto Institute of Technology, Japan, 2001.

[14] Mohiuddin Ahmad, M. S. Rahman, M. Z. Chowdhury, and M. Yamada, "Global optimization of optical flow technique on the computation of tissue-motion in cranial ultrasonographic movie," *Proc. of 2nd International Conference on Electrical Engineering (ICEE 2002),* 23-24 October, 2002, pp. 131 - 138.